REMAINING LIFE ASSESSMENT OF STEAM TURBINE AND HOT GAS EXPANDER COMPONENTS

by

Phillip Dowson

General Manager, Materials Engineering

Wenchao Wang

Senior Materials Engineer

Elliott Company

Jeannette, Pennsylvania

and

Agustin Alija

Maintenance Engineer

Dow Chemical PBBPolisur

Bahia Blanca, Argentina

Phillip Dowson is General Manager, Materials Engineering, with Elliott Company, in Jeannette, Pennsylvania, and has 34 years of experience in the turbomachinery industry. He is responsible for the metallurgical and welding engineering for the various Elliott product lines within the company. He is the author/coauthor of a number of technical articles related to topics such as abradable seals, high temperature corrosion, fracture mechanics, and welding/brazing of impellers.

Mr. Dowson graduated from Newcastle Polytechnic in Metallurgy and did his postgraduate work (M.S. degree) in Welding Engineering. He is a member of ASM, ASTM, and TWI.

Wenchao Wang is a Senior Materials Engineer with Elliott Company, in Jeannette, Pennsylvania. He joined the company in 1997, and has been involved in materials' related R&D projects, production supports, and aftermarket services. He is experienced in turbomachinery failure analysis, protective/functional coatings, and remaining life assessment.

Dr. Wang received a B.S. degree (Metallurgical Engineering, 1984) from the University of Science & Technology Beijing, and M.S. (1994) and Ph.D. (1997) degrees (both in Materials Science & Engineering) from the University of Cincinnati. He is a member of ASM.

Agustin Alija is a Maintenance Engineer of the Hydrocarbon and Energy Business of PBBPolisur (a Dow Chemical owned company), in Bahia Blanca, Argentina. He joined the company in June 2003.

Mr. Alija has a B.S. degree (Mechanical and Aeronautical Engineering, 2000) from the National University of Cordoba in Argentina.

ABSTRACT

In today's marketplace, a large percentage of oil refinery, petrochemical, and power generation plants throughout the world have been trying to reduce their operation cost by extending the service life of their critical machines, such as steam turbines and hot gas expanders, beyond the design life criteria. The key ingredient in plant life extension is remaining life assessment technology. This paper will outline the remaining life assessment procedures, and review the various damage mechanisms such as creep, fatigue, creep-fatigue, and various embrittlement mechanisms that can occur in these machines. Also highlighted will be the various testing methods for determining remaining life or life extension of components such as high precision stress relaxation (STR) test, which determines creep strength, and constant displacement rate (CDR) test, which evaluates fracture resistance. Other tests such as replication/microstructure analysis and toughness tests will also be reviewed for calculating the remaining life or life extension of the components. Use of the latest computer software will also be highlighted showing how creep-life, fatigue-life, and creep/fatigue-life calculations can be performed. Also shown will be actual life extension examples of steam turbines and hot gas expander components performed in the field.

INTRODUCTION

In recent years, from oil refinery to petrochemical and power generation industries, more and more plants throughout the world are facing a common issue—aging turbines, usually over 30 years old. Questions bearing in managers' minds are what is the machine condition and whether they can be continually operated (if yes, how long). The answer is significant not only for safety concerns but also for cost reduction, especially with today's limited budgets. Therefore, there is an increasingly strong desire for the engineering aftermarket service to perform "remaining life assessment" of steam turbines and hot gas expanders.

Remaining life assessment is to use metallurgical and fracture mechanics methodologies to predict the remaining life of structures and components that have been in service for an extended period of time, usually close to or beyond the designed life. Traditionally, if parts are found with material degradations or damages during an overhaul, they might be scrapped and replaced for risk-free consideration; even though they might have some useful life. Remaining life assessment offers a possible tool to estimate the useful remaining lifetime and avoid premature scrapping of the parts. So remaining life assessment is considered

to be an attractive method/process for cost reduction and reduction downtime.

Remaining life assessment has often been improperly referred to as "life extension." Actually this analysis cannot extend the lifetime of the components. It can only assess the useful remaining lifetime, based on the metallurgical examinations and theoretical (fracture mechanics) calculations. If such assessments indicate the need for extensive replacements and refurbishments, life extension may not prove to be a viable option. Above and beyond this objective, remaining life assessment technology serves many other purposes. It helps in setting up proper inspection schedules, maintenance procedures, and operating procedures. It should, therefore, be recognized at the outset that development of techniques for remaining life assessment is more enduring in value and broader in purpose than simply the extension of plant life. For instance, it has been possible to extend the inspections from six to 10 years for modern rotors, on the basis of assessments based on fracture mechanics, resulting in considerable savings.

In implementing remaining life assessment procedures, the appropriate failure definition applicable to a given situation must be determined at the outset, and the purpose for which the assessment is being carried out must be kept in mind. While determining the feasibility of extended plant life may be one objective, a more common objective is the setting of appropriate intervals for inspection, repair, and maintenance. In this context, remaining life assessment procedures are used only to ascertain that failures will not occur between such intervals. It should never be assumed that having performed a remaining life assessment study for a 20-year life extension, one could then wait for 20 years without interim monitoring. Periodic checks to ensure the validity of the initial approach are essential. In this sense, remaining life assessment should be viewed as an ongoing task, rather than a one-time activity.

A phased approach, in which the initial level includes nonincursive techniques followed by other levels of actual plant monitoring, then followed by nondestructive inspections and destructive tests would be the most logical and cost-effective approach. In Level I, assessments are performed using plant records, design stresses and temperatures, and minimum values of material properties from the original equipment manufacturer (OEM). Level II involves actual measurements of dimensions, temperatures, simplified stress calculations, and inspections coupled with the use of minimum material properties from the OEM. Level III involves indepth inspection, stress levels, plant monitoring, and generation of actual material data from samples removed from the component (destructive testing). The degree of the detail and accuracy of the results increases from Level I to Level III, but at the same time, the cost of the assessment also increases. Depending on the extent of the information available and the results obtained, the analysis may stop at any level or proceed to the next level as necessary.

In evaluating the failure criteria or remaining life, one needs to understand the various failure mechanisms that can occur. In turbomachinery components, the failure criteria can be governed by one or a combination of the following failure mechanisms:

- Fatigue—high cycle or low cycle
- Corrosion/corrosion fatigue
- Stress corrosion cracking (SCC)
- Erosion—solid particle or liquid impingement
- Erosion corrosion
- Embrittlement
- Creep rupture/creep fatigue
- High temperature corrosion/embrittlement
- Mechanical (foreign objective) damage

However, in remaining life assessment, usually only those mechanisms depending on temperature and time are taken into account. For example, for turbine casing, engineers usually focus on thermal stress-induced low cycle fatigue, creep rupture, and tempering embrittlement cracking. These failures usually are slow processes, therefore, they can be assessed and forecasted by examining the warning evidences in the material.

Countless works have been done to study the behaviors of fatigue crack initiation/propagation and creep or embrittlement rupture in steels and alloys. Scientists and engineers have reached such a level that, by knowing the flaw size or microstructure deterioration/damage, one can theoretically calculate and predict the remaining lifetime of the parts, based on the knowledge of the material properties and understanding of the stress distributions.

FATIGUE

Failures that occur under cyclic loading are termed fatigue failures. These can be vibration stresses on blades, alternating bending loads on shafts, fluctuating thermal stresses during start-stop cycles, etc. There are two types of fatigue: low cycle fatigue (LCF), high cycle fatigue (HCF). Traditionally, low cycle fatigue failure is classified occurring below 10^4 cycles, and high cycle fatigue is above that number. An important distinction between HCF and LCF is that in HCF most of the fatigue life is spent in crack initiation, whereas in LCF most of the life is spent in crack propagation because cracks are found to initiate within three to 10 percent of the fatigue life. HCF is usually associated with lower stress, while LCF usually occurs under higher stress.

Remaining life of casings or rotating components is generally based upon crack growth consideration. Fracture mechanics is the mathematical tool that is employed. It provides the concepts and equations used to determine how cracks grow and their effect on the strength of the structure. At the authors' company fracture mechanics is utilized in analyzing the structural integrity of components that have been in operation to determine whether the component is suitable for further operation. Based upon crack growth analysis one considers a number of scenarios.

From an initial defect size a_o one must determine critical flaw size a_c for fast fracture.

$$\begin{aligned} a_o &\rightarrow a_c \\ K_I &\rightarrow K_{IC} \end{aligned} \tag{1}$$

where:

K_I = Applied tensile mode I stress intensity factor
K_{IC} = Plane strain fracture toughness of material

For LCF, determine how many cycles for a_o to grow to a_c. For HCF, one must prevent crack growth. Consequently for HCF, $\Delta K_I < \Delta K_{th}$, where:

ΔK_I = Stress intensity factor range ksi$\sqrt{inch}$
ΔK_{th} = Threshold stress intensity factor range below which fatigue crack growth (or corrosion fatigue crack growth) does not occur

Further discussion of fracture mechanic concepts can be found elsewhere (Dowson, 1995, 1994).

CREEP RUPTURE AND STRESS RUPTURE

Evidence of creep damage in the high temperature regions of blade attachment areas of rotors has been observed in some instances (Bush, 1982). The rim stresses and metal temperature at these locations are assessed against the creep rupture data for that particular grade of steel/or material. Traditionally one has used a Larson-Miller (LM) plot of the type shown in Figure 1.

The degree of safety margin depends on the user and what lower bound design curve is applied. Since these curves are based upon the chemistry, variation in chemistry for a particular grade can have an effect on the Larson-Miller curve. Also, Larson-Miller

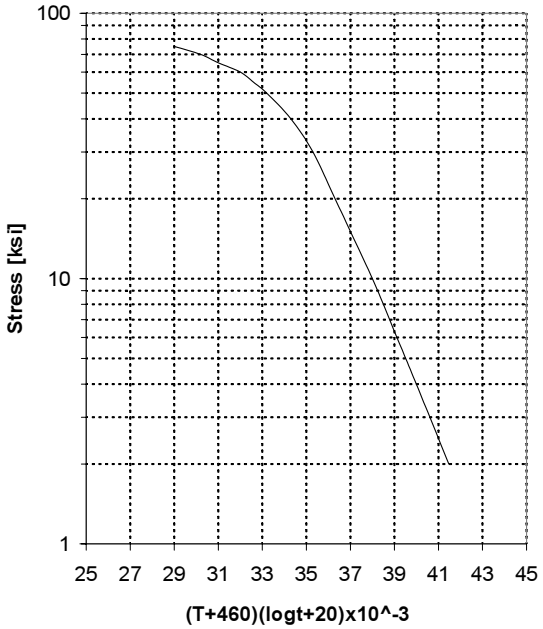

Figure 1. Larson-Miller Curve of Cr-Mo-V Alloy Steel (ASTM A470 Class 8).

curves are generally based upon creep rupture tests done for 10^4 to 3×10^4 hours and very few data at 10^5 hours. Consequently, the data for longer hours are generally extrapolated. Since most of the creep rupture data is done with smooth bar specimens, the effect of notch ductility at long-term service has not been done. Short-term notched bar tests may fail to predict the onset of notch sensitivity. Notch sensitively is not an inherent property but depends on the temperature, stress, stress state, and strain rate.

In assessing remaining life of the components due to creep, such as blade attachments, crack initiation is used as the criterion. However, with the emergence of cleaner steel and fracture mechanics and an increasing need to extend the life of a component, application of crack growth techniques have become common in the past decade.

For crack initiation as the fracture criterion, history-based calculation methods are often used to estimate life.

Methods for Crack Initiation Due to Creep

For the analytical method, one must have accurate operating history of the components, which may consist of temperature, applied loads, changes in operation, such as shut downs or variation in speed or pressure. A simplistic estimation of the creep life expended can be made by assessing the relaxed long-term bore stresses and rim stresses against the standard rupture data using the life fraction rule. The life fraction rule (LFR) states that at failure:

$$\sum \frac{t_i}{t_{ri}} = 1 \qquad (2)$$

where t_i is the time spent at a given stress and temperature and t_{ri} is the rupture life for the same test conditions.

- Example:

The purpose of this example is to illustrate the use of the life-fraction rule. A steam turbine piping system, made of 1.25Cr-0.5Mo steel designed for a hoop stress of 7 ksi, was operated at 1000°F (538°C) for 42,500 hours and at 1025°F (552°C) for the next 42,500 hours. Calculate the life fraction expended using the life fraction rule. From the Larson-Miller parameter curve of the steel, it is found that, at σ = 7 ksi,

t_{ri} at 1000°F = 220,000 hours
t_{ri} at 1025°F = 82,380 hours

Life fraction expended, t_i/t_{ri}, at 1000°F

$$= \frac{42{,}500}{220{,}000} = 0.19$$

Life fraction expended, t_i/t_{ri}, at 1025°F

$$= \frac{42{,}500}{82{,}380} = 0.516$$

The total life fraction expended is 0.71.

This rule was found to work well for small changes in stress and temperature especially for CrMoV rotor steel. However, for stress variations, the actual rupture lives were lower than the predicted values. Consequently, the LFR is generally valid for variable-temperature conditions as long as changing creep mechanisms and environmental interaction do not interfere with test results. However, the possible effect of material ductility on the applicability of the LFR needs to be investigated.

Nondestructive Techniques

Conventional nondestructive evaluation (NDE) techniques fail to detect incipient damage that can be a precursor to crack initiation and subsequent rapid failure. However, there are other NDE techniques that have been developed for estimating the life consumption. These include microstructural techniques and hardness based techniques.

Metallographic Examination

Metallographic techniques have been developed that can correlate changes in the microstructure and the onset of incipient creep damage, such as triple point cavitation at the grain boundaries. For this technique, measurements by replication technique are taken on crack sensitive areas that are subjected to the higher temperatures and stresses. These areas are generally indicated by experience and analysis of previous damages.

The creep damage measured by replication is classified into four damage stages:

- Isolated cavities (A)
- Oriented cavities (B)
- Macrocracks (linking of cavities) (C)
- Formation of macrocracks (D)

Figure 2 shows the location of the four stages on the creep strain/exposure time curve (Neubauer and Wadel, 1983).

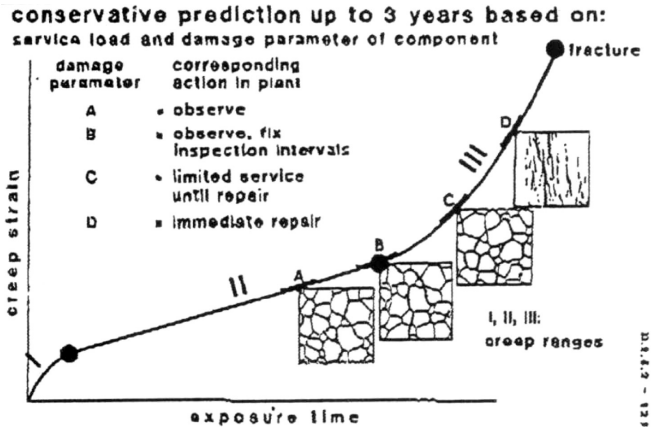

Figure 2. Replicas for Remaining Life Assessment.

In applying this approach Neubauer and Wadel (1983) classified the stages into five stages, which are Undamaged, Stage A, Stage B, Stage C, and Stage D. These stages corresponded roughly to expended life fracture ($t/_{tr}$) values of 0.27, 0.46, 0.65, 0.84, and 1, respectively, using the conservative lower bound curve.

Consequently, the remaining life can be calculated using the relationship as shown in Equation (3):

$$t_{rem} = t\left(\frac{t_r}{t} - 1\right) \tag{3}$$

where t is the service life expended and t_r is the rupture life.

For undamaged material and damaged stages A, B, and C, the remaining life was found to be approximately 2.7t, 1.17t, 0.54t, and 0.19t, respectively. Then by applying a safety factor of 3 to the calculations, the safe reinspection intervals will become 0.9t, 0.4t, 0.18t, and 0.06t, respectively. This approach has been developed and implemented in the power generation industry (Viswanathan and Gehl, 1991). It was found to give increased inspection intervals as compared to the Neubauer and Wadel (1983) approach, as shown in Table 1.

Table 1. Suggested Reinspection Intervals for a Plant with 30 Years of Prior Service.

	Inspection Interval (Years)	
Damage Classification	**Wedel-Neubauer**	**EPRI-APTECH**
Undamaged	5	27
A. Isolated Cavities	3	12
B. Oriented Cavities	1.5	5.4
C. Linked Cavities (Microcracks)	0.5	1.8
D. Macrocracks	Repair Immediately	Based on fracture mechanics

This approach has been applied by several utilities and realized significant savings in inspection costs. Other investigations indicate that there are wide variations in behavior due to differences in grain size, ductility, and impurity control (Carlton, et al., 1967). For conservatism, the authors' company adapted the Neubauer and Wadel (1983) approach and classified the five stages as follows:

1. Undamaged material—Equipment can run and be reinspected at next shutdown.
2. Class A—Reinspection would be three to five years.
3. Class B—Reinspection would be one and one-half to three years.
4. Class C—Replacement or repair would be needed within six months.
5. Class D—Immediate replacement or repair would be required.

Hardness Measurement

The first attempt to develop hardness as a technique to determine creep damage was by Goldhoff and Woodford (1972). In their study a good correlation was observed between room temperature hardness measured on exposed creep specimens and the post exposure rupture life (Figure 3).

If similar calibration could be established between prior creep life expended or the remaining life fraction in the post exposure test and the hardness values for a range of CrMoV steels, this method could be applied to estimation of remaining life. However, data of this nature are not available in sufficient quantity. Other work done by Viswanathan and Gehl (1992) showed a lot of promise where they attempted to use the hardness technique as a stress indication. They observed that the application of stress accelerated the softening process and shifted the hardness to lower parameter values compared with the case of simple thermal softening on a plot of hardness versus a modified Larson-Miller parameter (Figure 4).

Destructive Techniques

Newer tests to ascertain the useful life of used and/or repaired components have been utilized by the authors' company. Design-for-performance is a recently developed methodology for evaluating the creep strength and fracture resistance of high temperature materials. Whereas the traditional approach to creep design involves

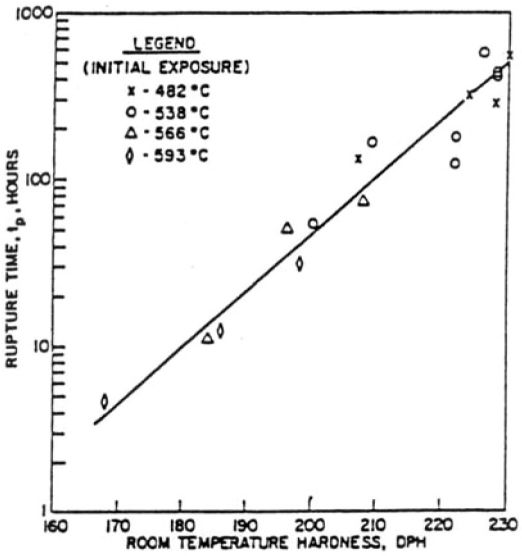

Figure 3. Correlation Between Post-Exposure Rupture Time in the Standard Test at 538°C (1000°F) and 240 MPa and Room Temperature Hardness for Cr-Mo-V Rotor Steel.

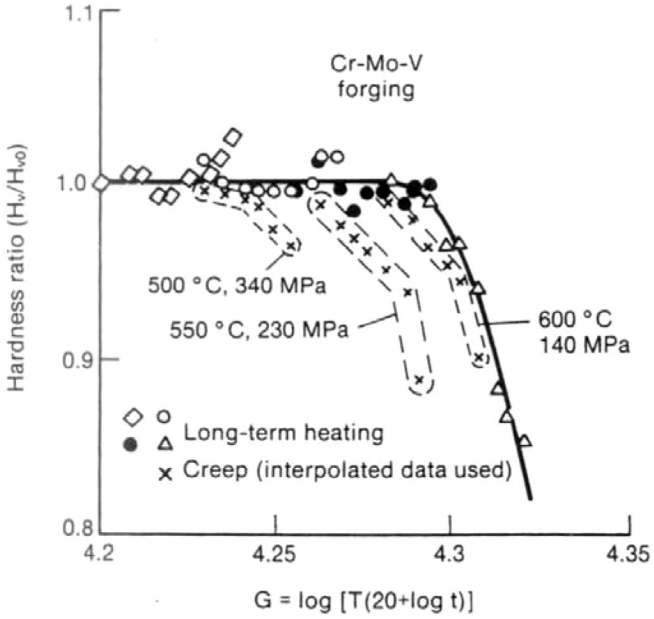

Figure 4. Plot of Hardness Ratio Versus G Parameter for Long-Term Heating and Creep of Cr-Mo-V Rotor Steel.

long-term testing and attempts to incorporate microstructural evolution in the test measurements, the new approach aims to exclude these changes in a short time high-precision test. The test may also be used to evaluate consequences of such changes in service-exposed samples. The new methodology recognizes that separate tests are necessary to measure creep strength and fracture resistance. For creep strength, a stress versus creep rate response is determined from a stress relaxation test (SRT), and for fracture resistance a constant displacement rate (CDR) test of a notched temple specimen is performed at a temperature where the part is most vulnerable to fracture (Woodford, 1993).

Constant Displacement Rate Test

A description of the standardized CDR test is found elsewhere (Pope and Genyen, 1989). The data from the CDR test are tabulated in a curve similar to the load displacement curve for an

ordinary elevated tensile test. For a typical tensile test fracture becomes unstable after the peak load is reached. On the other hand, in the CDR test, since the deformation is controlled at a constant rate and the notch is midway between the controlling extensometer, fracture rarely becomes unstable.

For a valid CDR test, the criterion for failure was considered to be the value of "displacement at fracture," defined as the point of intersection of the 100 pound load line and the descending load displacement curve. The "displacement at failure" is measured from the start of the test to the point where the load displacement curve decreases below 100 pounds (Figure 5).

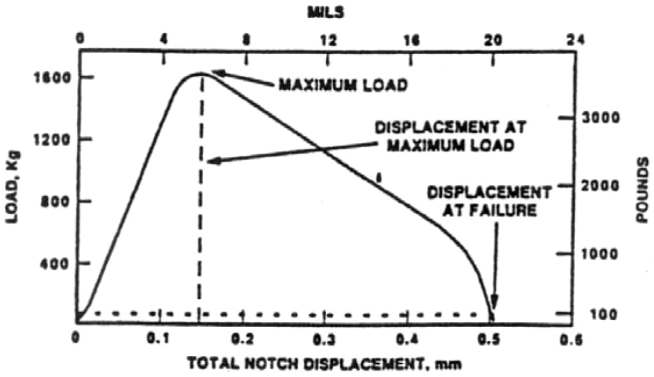

Figure 5. Example of Load Displacement Curve from CDR Tests at 1200°F and 2 mils/in/hr.

An example of how the environment can affect the notch sensitivity of the material is indicated by Figure 6. This example illustrates the effect of air exposure on IN738.

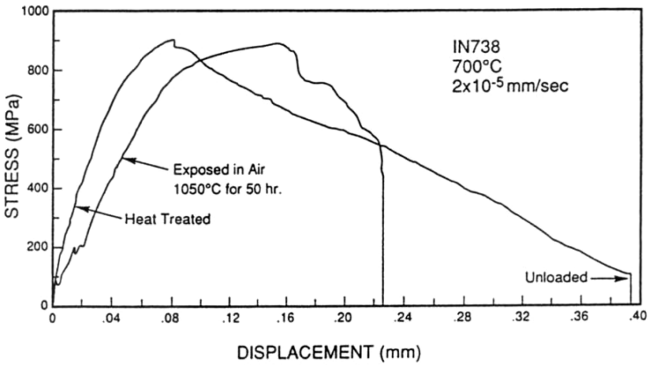

Figure 6. Constant Displacement Rate Tests Comparing Crack Growth Resistance in Heat Treated and Oxygen Embrittled Specimens.

Stress Relaxation Test

Specially designed samples were tested on an electromechanical test system fitted with self-aligning grips, a 1500°C (2732°F) short furnace, and a capacitive extensometer. Details of the specimen geometry and extensometer sensitivity are provided elsewhere (Woodford, et al., 1992).

The standard test procedure involved loading the specimen at a fast rate of 10 MPa/sec (1450 psi/sec) to a prescribed stress and then switching to strain control on the specimen and monitoring the relaxation stress. The inelastic (principally creep) strain-rate is calculated from the following equations, Equations (4) and (5).

$$\varepsilon_e + \varepsilon_I = \varepsilon_t = Cons\tan t \tag{4}$$

$$\dot{\varepsilon}_I = -\dot{\varepsilon}_e = -\frac{1}{\mathrm{E}}\frac{d\sigma}{dt} \tag{5}$$

Where ϵ_e is the elastic strain, $\dot{\epsilon}_e$ is the elastic strain rate, ϵ_I is the inelastic strain (principally creep strain), $\dot{\epsilon}_I$ is the inelastic strain rate, ϵ_t is the total strain, σ is the stress, and E is the elastic modulus measured during loading. Using this procedure, stress versus strain-rate curves were generated covering up to five orders of magnitude in strain-rate in a test lasting less than 5 hours.

An example of the data generated in such tests is provided in Figure 7 for Waspaloy® material. This shows stress versus predicted time to 1 percent creep for Waspaloy®. By utilizing these data one can plot a stress versus Larson-Miller parameter for 1 percent predicted creep of Waspaloy® compared to rupture data (Figure 8). From the data shown on the curve, the stress relaxation test can generate creep-stress rupture data in less than a few weeks as compared to the traditional approach that incorporates long time testing.

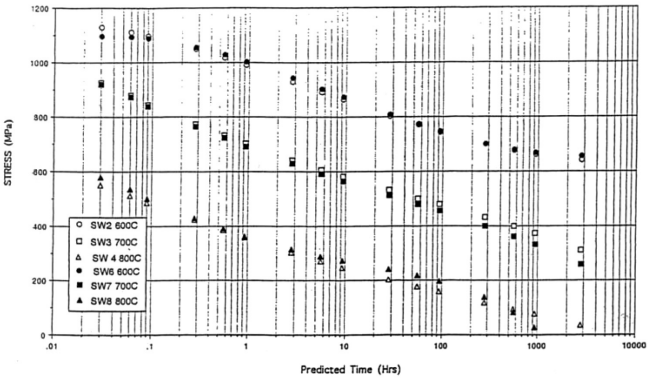

Figure 7. Stress Versus Predicted Times to 1 Percent Creep for Standard Waspaloy®.

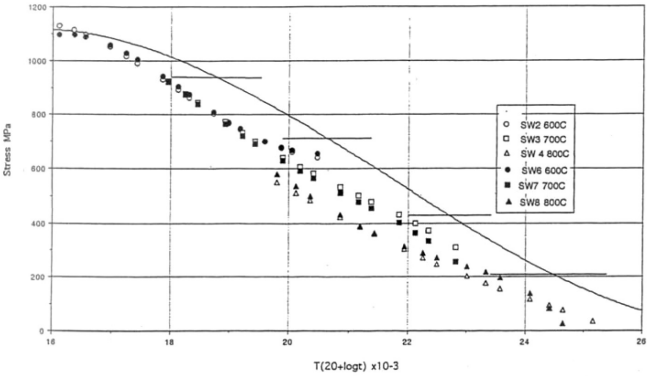

Figure 8. Stress Versus Larson-Miller Parameter for 1 Percent Predicted Creep of Standard Waspaloy® Compared with Rupture Data.

One major objective to this framework has been that effects of very long time exposures that could influence stress rupture life will not be accounted for. However, Woodford believes that such effects, i.e., precipitation of embrittling phases and grain boundary segregation of harmful elements, are expected to influence the fracture resistance rather than creep resistance. The authors' company has utilized this methodology to generate data for high temperature materials and weldments. Current methods are being developed for miniature specimens taken from serviced blades. From these data, it is envisioned that establishment of a set of minimum performance criteria will enable repair/rejuvenation/replacement decisions to be made.

CREEP/FATIGUE INTERACTION

For components that operate at higher temperature where creep growth can occur, one must take into account the creep crack growth at intervals during the fatigue life of the component. The following is an example of a high temperature steam turbine rotor

that failed catastrophically at a power plant in Tennessee (Saxena, 1998). The authors utilized the latest computer software to demonstrate how creep-life, fatigue life, and creep/fatigue-life calculations can be performed, and how inaccurate the calculation would be without accounting for the creep life.

The power plant rotor was operated for 106,000 hours and had incurred 105 cold starts and 183 hot starts. The material was 1CR-1Mo-0.25V forging and had been operating at a temperature of 800°F. The cracks originated from several majority node set (MnS) clusters with the original flaw size of 0.254 inch × 5.51 inch and 0.7 inch from the bore of the rotor (Figure 9).

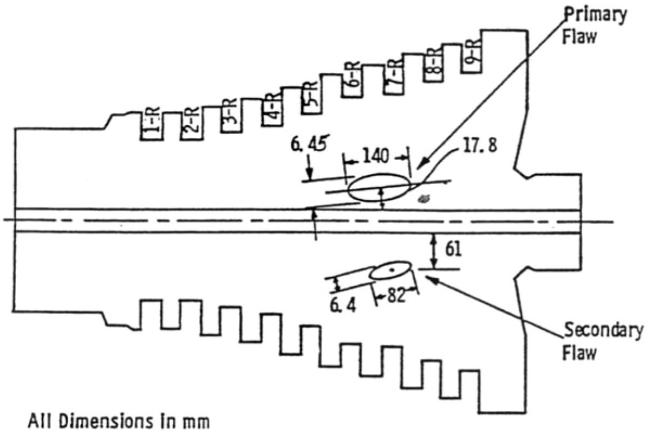

Figure 9. Schematic of the Intermediate Pressure (IP) Section of the Rotary Showing the Size and Location of the Primary and Secondary Flaws Beneath the Seventh Row (7-R) of Blades.

Step 1—Assessment of Low Cycle Fatigue Life

The principle is that fatigue crack growth follows equations such as the Paris law:

$$\frac{da}{dN} = C_f \Delta K^{n_f} \tag{6}$$

C_f and $^{n}{}_{f}$ are constants that depend on the material and environment.

The stress intensity factor range ΔK depends on the stress level at the crack tip. The life assessment criterion is that critical crack size a_c is not to be exceeded. In other words,

$$a \le a_c \tag{7}$$

Figure 10 and Figure 11 show the stress intensity factor calculation together with the crack model that was used.

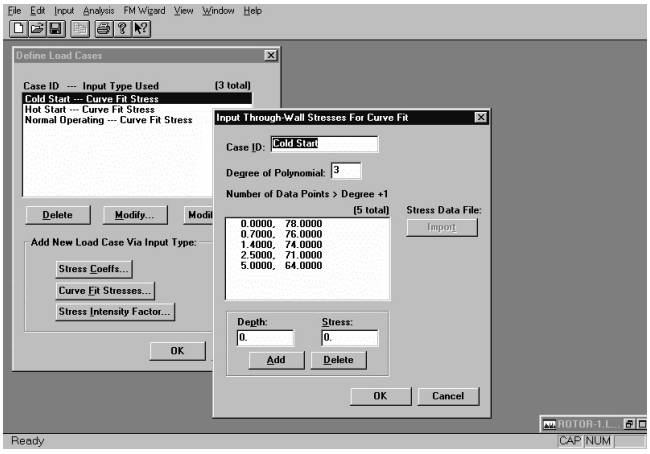

Figure 10. Computer Software Module. Stress Intensity Factor Calculation.

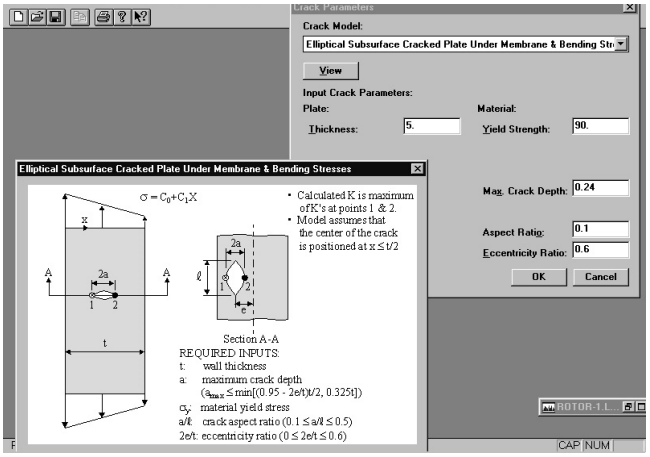

Figure 11. Computer Software Model—Elliptical Subsurface Cracked Plate under Membrane and Bending Stresses.

By computing the information a plot of stress intensity factor versus crack depth was done. Based on the plane strain fracture toughness of the material, the critical crack size 0.42 inch for cold start and 0.48 inch for hot start were determined (Figure 12).

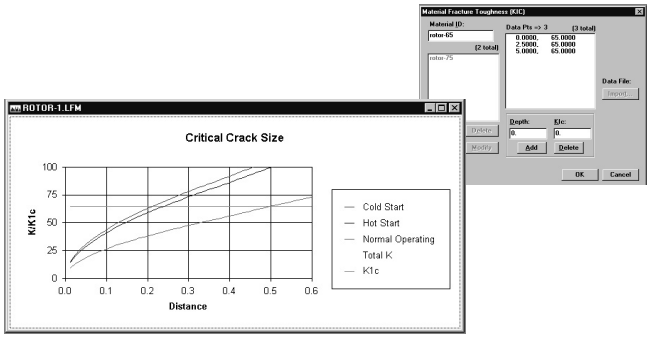

Figure 12. Critical Crack Size Calculation—The Critical Crack Size a_c is 0.42 Inch for Cold Start and 0.48 Inch for Hot Start.

Fatigue crack growth using the Paris law was computerized (Figure 13, Figure 14) and the low cycle fatigue crack growth was determined for both cold and hot starts. Figure 15 shows the low cycle fatigue crack growth, which does not compare very well with that of the real life.

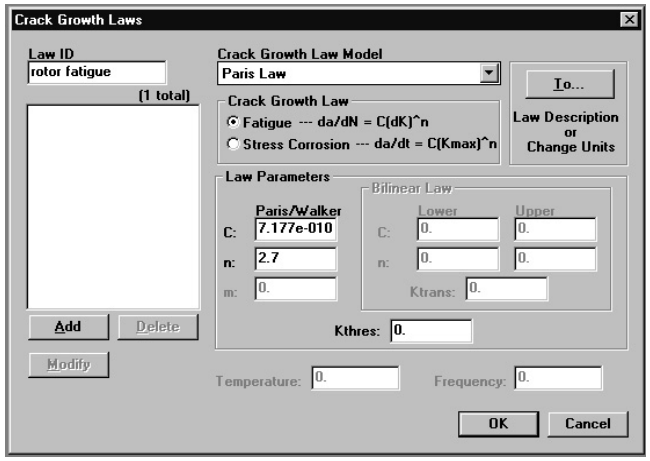

Figure 13. Fatigue Crack Growth.

The reason for the calculated life being much longer than the real life is that the hold time effect (or creep cracking effect) is not

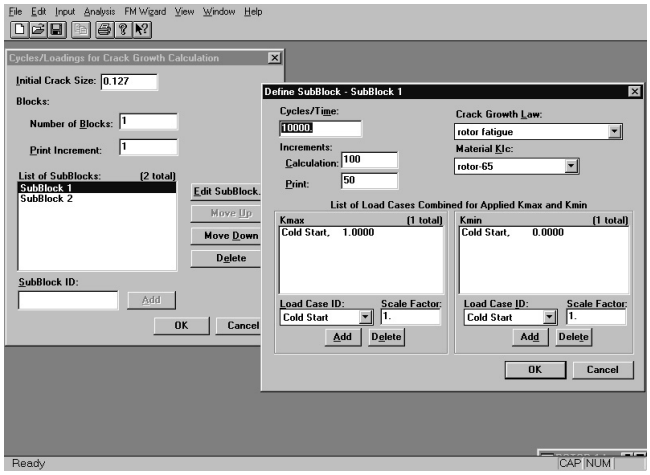

Figure 14. Fatigue Crack Growth Calculation Model.

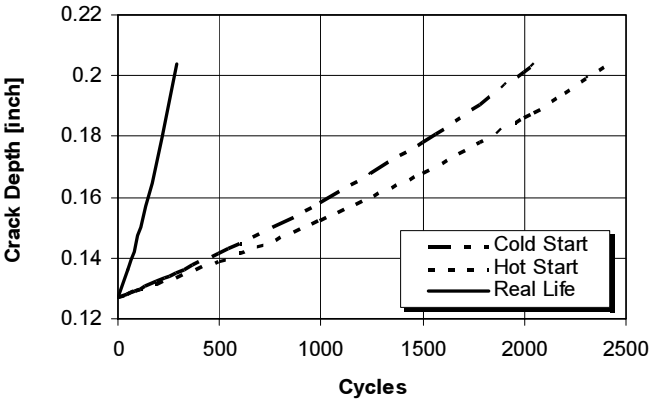

Figure 15. Shows Low Cycle Fatigue Crack Growth for Cold and Hot Starts Compared to Real Life.

taken into account. Consequently, one must run a creep-fatigue remaining life assessment. The principle is that high temperature crack propagation is the summation of high temperature fatigue plus primary creep plus secondary creep.

Creep-fatigue crack growth:

$$\frac{da}{dt} = \underbrace{C_c\left[C_t(t)\right]^q}_{Creep} + \underbrace{\frac{C_f}{h}(\Delta K)^{n_f}}_{Fatigue} \tag{8}$$

where h is the hold time in each cycle (which is 368 hours in this case). The creep crack driving force consists of two parts:

$$C_t(t) = \underbrace{\left[C^*\right]^{2/[(1+p)(m-1)]}\left[\frac{\left(1-\nu^2\right)K^2}{E(n+1)t}\right]^{1-2/[(1+p)(m-1)]} + \frac{n+p+1}{(n+1)(p+1)}C_h^*\left(\frac{1}{t}\right)^{p/(p+1)}}_{PrimaryCreep} \underbrace{+C^*}_{SecondaryCreep} \tag{9}$$

The data that are input into the code are shown in Figure 16 and Figure 17. The calculation shows that, accounting for creep effect, the creep-fatigue growth is much closer to the real life (Figure 18).

This example demonstrates that if the material/component is operating in the creep mode, one must perform a creep-fatigue analysis instead of fatigue only. Generally a rule of thumb is that if only low cycle fatigue crack growth is counted and creep is not, then the calculated lifetime is about 10 times longer than the real life. By utilizing this software program, more accurate remaining life assessment can be achieved for materials operating in the creep regime under cyclic loading. Also, the lesson being learned is that this rotor should have been examined by ultrasonic inspection every five years.

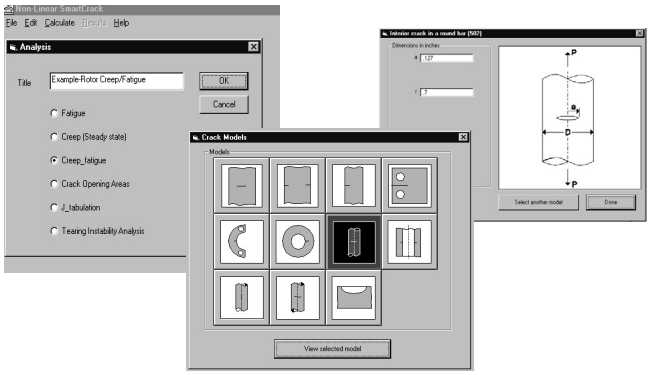

Figure 16. Creep/Fatigue Model.

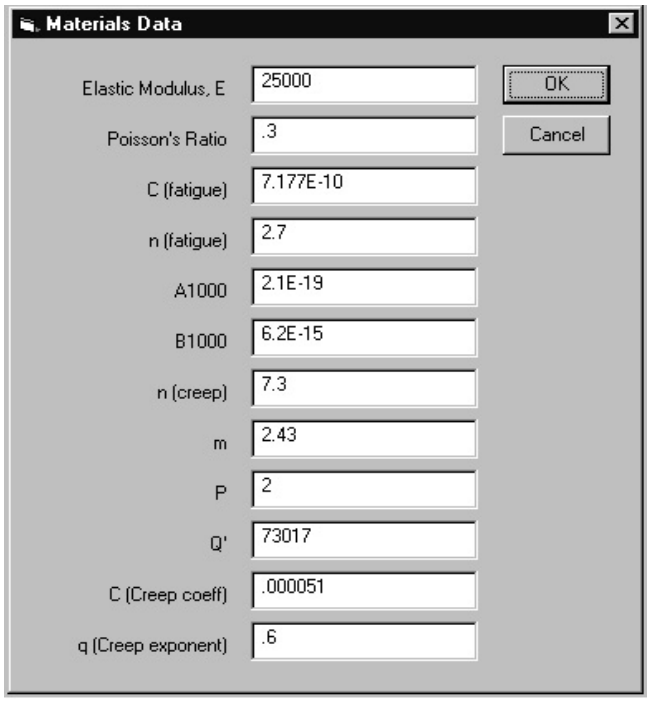

Figure 17. Creep/Fatigue Material Data.

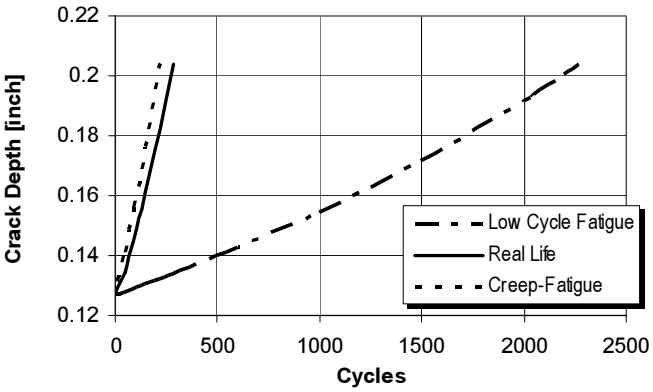

Figure 18. Compares Low Cycle Fatigue and Creep-Fatigue Crack Growth to the Real Crack Growth.

EMBRITTLEMENT

Trends toward increasing size and operating stresses in components, such as large turbine-generator rotors, require higher hardenability steels with increased strength and fracture toughness. However, higher hardenability steels especially those containing

nickel and chromium are usually much more susceptible to a phenomenon called temper embrittlement. The term temper embrittlement refers to a shift in the brittle-to-ductile transition temperature when steels/rotor shafts are heated or cooled slowly through the temperature range of 660°F to 1060°F. This shift in the brittle-to-ductile transition temperature can be reversed by heating at a temperature of 1100°F or higher then fast cooled. Consequently, when examining rotor or casings that have been in service and operated within this temper embrittlement temperature range, the property toughness becomes an important criterion.

Evaluation of Toughness

Due to the advancement of fracture mechanics, it has now become possible to characterize toughness in terms of critical flaw size a_c. The definition of a_c depends on the conditions under which final rapid fracture occurs following the initial phase of subcritical crack growth. At rotor grooves and rotor bores where final fracture is likely to occur at low temperatures during start-stop transients, a_c is dictated by linear elastic fracture mechanics. a_c is given by an expression of the form:

$$K_{IC} = M\sigma\sqrt{\pi a_c} \tag{10}$$

where K_{IC} is the fracture toughness of the material or critical stress intensity for fracture, M is a constant to a given flaw size and geometry, and σ is the nominal applied stress.

A typical loading sequence for turbine rotors shows variation in temperature and stress and their effect on critical flaw size a_c for cold start sequence (Viswanathan and Jaffee, 1983). Figure 19 shows the cold start sequence and associated variations in stress (σ), temperature (T), and critical flaw size (a_c) as a function of time for the power plant rotor, which failed catastrophically.

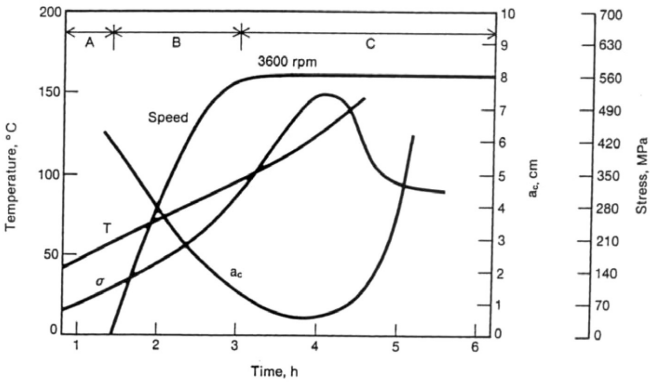

Figure 19. Illustration of Cold-Start Sequence and Associated Variations in Stress (σ), Temperature (T), and Critical Flaw Size (a_c) as Functions of Time from Start.

Region A consists of a warmup period after which the rotor was gradually brought up to speed (Region B). Once continuous operating speed was reached (Region C) approximately 3 hours after the warm up period, maximum loading was applied. Analysis of the failure location (seventh row) showed that stresses reached a peak value of 74 ksi (520 MPa), 1½ hours after the maximum continuous speed had been attained. The critical crack size reached its lowest value of 0.27 inch (6.9 mm) at a temperature of 270°F (132°C) and 74 ksi (510 MPa). Since variation in temperature, stress, and material fracture toughness at the defect location can dictate the a_c value for the rotor, one must calculate for the worst combination of these variables to prevent failure.

This can be done by using lower scatter band values of K_{IC}. However, to determine K_{IC} for rotors, large specimens need to be taken to satisfy the plane strain conditions required for a valid test. A more common practice is to determine the ductile-brittle fracture at transition temperature (FATT) using samples extracted from the periphery of a rotor and converting the FATT into K_{IC} using a correlation such as the one shown in Figure 20 (Schwant and Timo, 1985).

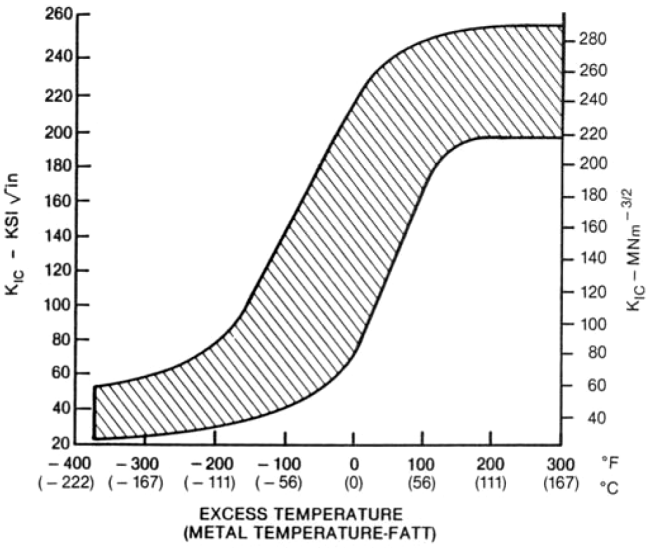

Figure 20. Turbine Rotor and Wheel Toughness Data.

Viswanathan and Gehl (1991) evaluated a number of data from numerous exposed CrMoV rotors and defined a lower threshold band for low alloy steels. The lower limit line for CrMoV steel is defined by the equation (Viswanathan and Wells, 1995) below:

$$K_{IC} = 95.042 + 0.5872T_E + 0.00168T_E^2 + 0.00000163 \tag{11}$$

where K_{IC} is expressed in ksi-(in) ½ and T_E is the excess temperature (T-FATT) expressed in degrees Fahrenheit. Once the FATT is known, a K_{IC} versus temperature T curve can be established and used to determine a_c versus T.

However, such procedures tended to be conservative and there have been various other nondestructive and relatively destructive tests involving removal of very small samples to determine toughness of rotors. These techniques investigated include eddy-current examination, analytical electron microscope, secondary ion mass spectroscopy (SIMS), compositional correlations, Auger electron spectroscopy, chemical etching, use of single Charpy specimen, and small punch tests. The techniques that show the most promise and have currently been applied in service application are:

- Correlation based on composition.
- Small punch testing.
- Chemical etching.

Correlation Based on Composition

An American Society for Testing and Materials (ASTM) special task force on large turbine generator rotors of Subcommittee VI of ASTM Committee A-1 on steel has conducted a systematic study of the isothermal embrittlement at 750°F of vacuum carbon deoxidized (VCD) NiCrMoV rotor steels. Elements, such as P, Sn, As, Sb, and Mo were varied in a controlled fashion and the shifts in FATT, (Δ) FATT were measured after 10,000 hours of exposure. From the results, the following correlations were observed in Equation (12):

$$\Delta FATT = 13544P + 12950Sn + 2100As - 93Mo - 810{,}000(P \times Sn) \tag{12}$$

where ΔFATT is expressed in degrees Fahrenheit and the correlation of all the elements are expressed in weight percent. According

to this correlation, the elements P, Sn, and As increase temper embrittlement of steels, while Mo, P, and Sn interaction decrease the temper embrittlement susceptibility.

All available 10,000 hour embrittlement data are plotted in Figure 21 as a function of calculated ΔFATT using Equation (11), (Newhouse, et al., 1972). A good correlation is observed between calculated and experimental ΔFATT. The scatter for these data is approximately ±30°F for 750°F exposure and ±15°F for the 650°F exposure.

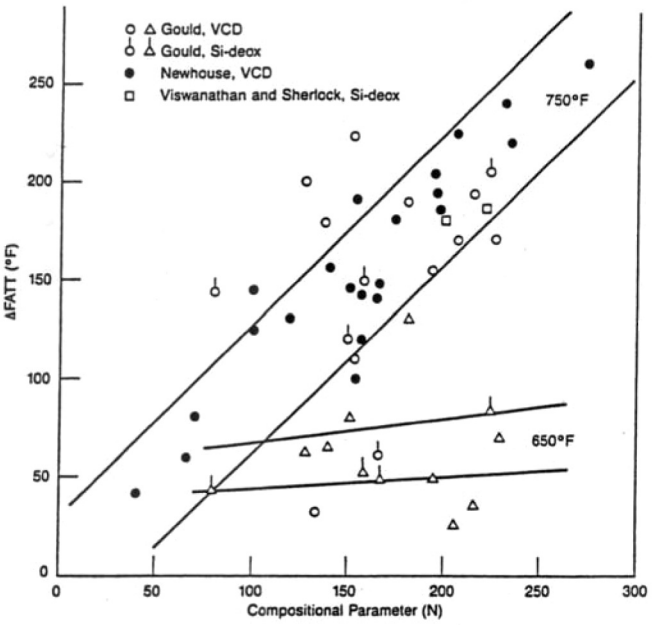

Figure 21. Correlation Between Compositional Parameter "N" and the Shift in FATT of NiCrMoV Steels Following Exposure at 650°F and 750°F for 8800 Hours.

Other correlations for determining the temper embrittlement susceptibility of steel, such as the J factor proposed by Watanabe and Murakami (1981) and $\bar{X}$ factor proposed by Bruscato (1970), are widely used.

These factors are given by:

$$J = (Si + Mn)(P + Sn)10^4 \tag{13}$$

$$\bar{X} = (10P + 5Sb + 4Sn + As)10^2 \tag{14}$$

The Figure 22 and 23 show the relationship between increase of FATT and J factor and $\bar{X}$ factor at 399°C (750.2°F) for a 3.5 percent NiCrMoV steel.

Small Punch Testing

Small punch testing of small disk-like specimens subjected to bending loads have found good correlation for determining the ductile-brittle transition temperature (Baik, et al., 1983). The procedure consists of thin plate 0.4 × 0.4 × 0.02 inch subjected to a punch deformation with a 0.09 inch diameter steel ball in a specially designed specimen holder. The test is performed at various temperatures and from the load deflector curves obtained at various temperatures, the fracture energy is calculated. The fracture energy is plotted as a function of test temperature to determine the ductile-to-brittle transition temperature. The area under the deflector curve denotes the energy absorbed during the test. This test procedure has been used successfully on a number of retired rotor samples to determine the T_{SP} (ductile-to-brittle transition) and found to correlate well with the Charpy FATT values (Foulds, et al., 1991) (Figure 24).

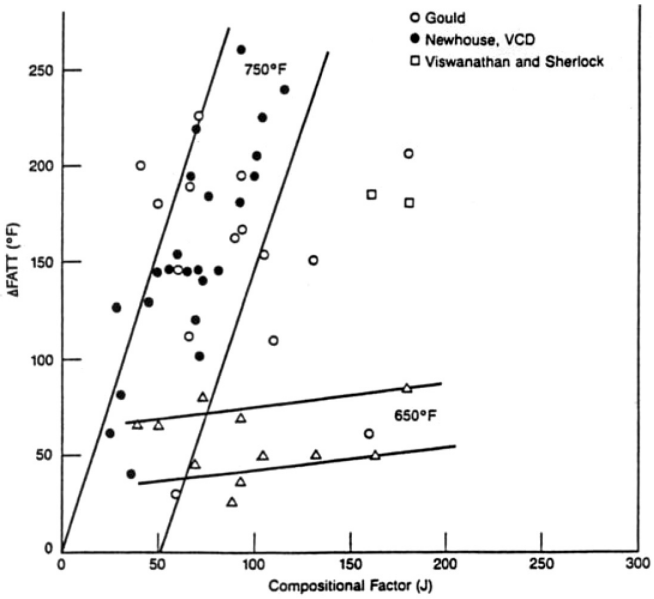

Figure 22. Correlation Between Compositional Factor "J" and the Shift in FATT of NiCrMoV Steels Following Exposure at 650°F and 750°F for 8800 Hours.

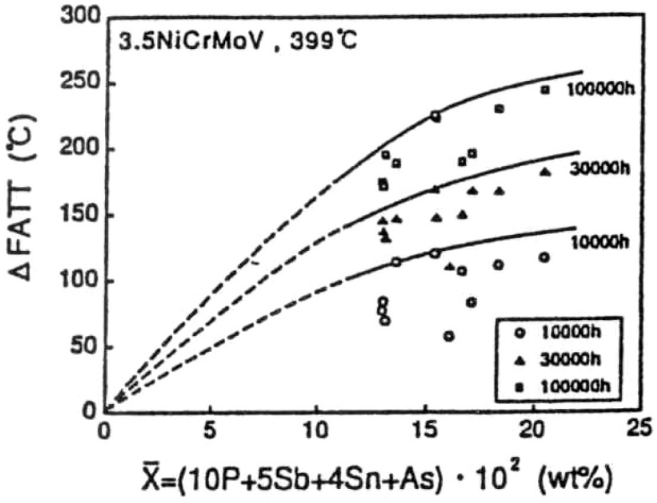

Figure 23. Relationship Between Increase of FATT and $\bar{X}$.

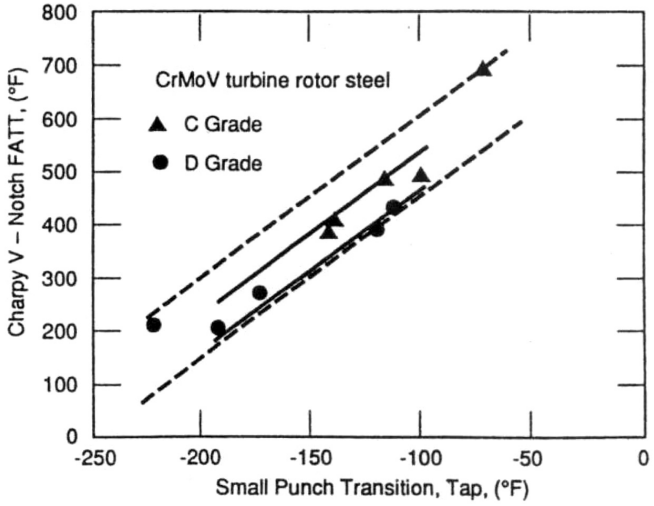

Figure 24. Correlation Between Charpy FATT and Small Punch Transition Temperature.

Chemical Etching

The grain boundaries of embrittled steel are attacked preferentially by picric acid solutions consisting of saturated picric acid solution with an addition of 1 gram of tridecyl/benzene sulfonate (per 100 ml of aqueous picric acid). Correlations have been made between the grain boundary groove depth as measured metallographically even from plastic replicas and the ΔFATT of the sample due to prior temper embrittlement. By using plastic replicas this technique becomes very attractive for field use (Kadoya, et al., 1991).

Also Kadoya, et al., (1991) were able to correlate the width of the grain boundary groove measured from plastic replicas using a scanning electronic microscopes (SEM), with the FATT of the samples and actual rotors. They also correlated the following equation based on regression analysis of a number of material variables. This equation was found to predict the FATT within a scatter of ±20°C.

$$FATT = 99.12W + 1.609H_V + 816.4Si + 6520Mn + 3320P + 310.4Cr + 3404Sn + 0.282J + 325.6 \quad (15)$$

where:
J is defined as (Si + Mn) (P + Sn) 10^4
W = Width of grain boundary groove
H_V = Vicker hardness of sample/rotor

By utilizing this equation, the calculated FATT values were compared with critical FATT values and the results were very attractive (Figure 25).

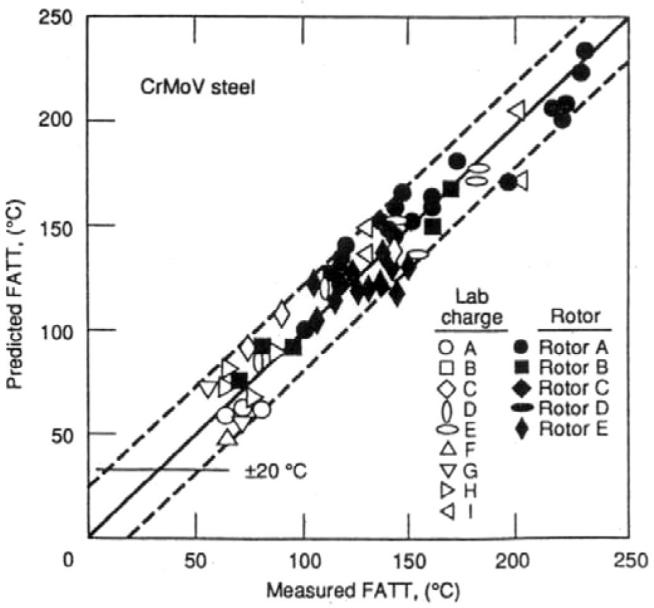

Figure 25. Comparison Between Measured FATT and Predicted FATT Using the Method of Etching.

HIGH TEMPERATURE CORROSION

Fluid catalytic cracking (FCC) hot gas expanders operate in environments that can be both corrosive and erosive. Although it is well documented that the source of erosion comes from the regenerated catalyst that is carried with the hot flue gas from the FCC, its effect on high temperature corrosion has only begun to be understood by the authors' company. Papers published by the author outline the relationship of stress and temperature on the high temperature corrosion/fracture mechanics of Waspaloy® in various catalyst environments (Dowson, et al., 1995; Dowson and Stinner, 2000).

The nature of the corrosion attack is primarily influenced by the type of crude oil stock, which in time has a bearing on the resulting flue gas composition, regenerated catalyst, and the nature and quality of additions injected into the FCC process.

When evaluating remaining life assessment of hot gas expanders especially the rotating components, one must consider the effect of the environment such as high temperature corrosion. The authors' company has developed a fracture mechanics model that incorporated both the effect of oxide wedge formation and the apparent reduction in fracture toughness of Waspaloy® in contact with the catalyst residue. By utilizing this model one can predict whether fracture will occur under various environmental/operating conditions of the hot gas expander. The authors' company periodically tests catalysts from end-users' hot gas expanders to determine if oxide wedge can occur and what life span to reach the critical size for failure. Generally, if the catalyst is active, then high temperature corrosion will occur. Consequently, a blade will be removed from the unit and examined metallographically to determine the oxide wedge depth. Based upon the depth and time of operation, the remaining life can be estimated (Figure 26).

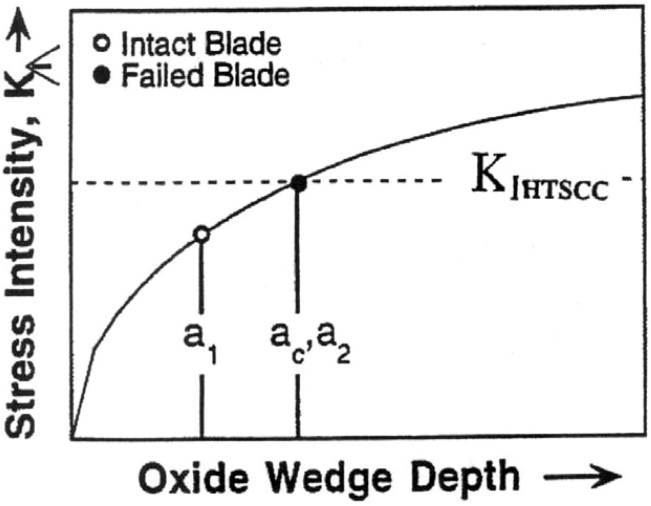

Figure 26. Stress Intensity Profile Versus Oxide Wedge Depth for Unit A. Critical Oxide Wedge Depth for Failure Was Defined as a_c. In the Failed Blade, a_2 Was Found to Exceed a_c. In an Intact Blade, a_1 Was Less Than a_c.

CASE STUDY 1— REMAINING LIFE ASSESSMENT OF STEAM TURBINE CASING

Background Information of the Turbines

The subject ethylene plant has three steam turbines that drive three trains of compressors on the main deck. The units are listed in the following. The three turbines were commissioned in August 1981. They have been using the same steam source and are operated in similar conditions (as summarized in Table 2). This case study only discusses the remaining life assessment of one of them, a seven-stage 14 MW steam turbine.

According to the plant logbook, in the past 23 years, the turbine was started/stopped 24 times, which are plotted in Figure 27. During the last 23 years of operation, only two failure incidents were recorded. The first one was a damage on the rotor, due to condensate inlet during the startup of the turbine in the late 1980s. The other was found in the latest turnaround in 2004, in which a blade failure and multiple cracks at steam balance holes were found on the sixth stage disk that was subject to repair. The casing never experienced any problem in the past. During the turnaround in 1995, a remaining life assessment was performed by Wiegand (1995), and the casing was found to be in a very good condition, as shown later in the top photo of Figure 30. The turbine component materials are listed in Table 3.

Table 2. Turbine Operating Conditions.

Designed Conditions			Actual Conditions	
Temperature, F (C)		Inlet Pressure,	Inlet Temperature,	Inlet Pressure,
Inlet	1st Stage Disk	psig (kg/cm^{2}g)	F (C)	psig (kg/cm^{2}g)
806 (430)	692 (367)	696 (48.9)	797 (425)	710 (50)

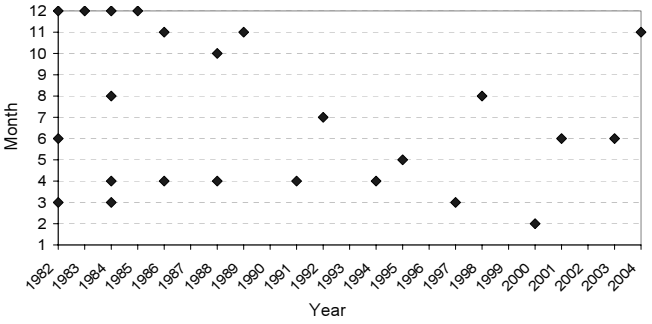

Figure 27. Turbine Start/Stop Record.

Table 3. Turbine Component Materials.

Steam-End Casing	Rotor Forging	Blades	Diaphragms
1.25Cr-0.5Mo alloy steel casting, ASTM A217 Grade WC6 (limited to 950 F service)	Ni-Mo-V alloy steel, ASTM A470 Class 4	AISI 403 stainless steel for all stages	Alloy steel plate ASTM A517 Grade F & A516 Grade 60 for 2nd to 5th stages. Gray cast iron ASTM A278 Class 40 for 6th & 7th stages.

Field Inspection

The turbine upper casing was visually examined. No cracks or reportable indications were found. The split-line bolt-holes were examined with dye-penetrant inspection, which did not reveal any cracks. The casing was polished at six different spots shown in Figure 28. The microstructure was observed with a portable optical microscope, and replicated for documentation (Figure 29). Microstructure deteriorations, such as carbide precipitation at grain boundaries and bainite degradation, were evident. However, the casing did not show any creep voids at any of the spots being examined. Hardness was measured at the same spots and the results are listed in Table 4.

Microstructure Deterioration of the Casings Material

In order to study the microstructure deterioration, a fragment of the sample being cut off from the casing was reheat treated to restore the original microstructure for comparison. The reheat treatment was done in two steps: normalized at 1685°F (918°C) for 1 hour and controlled air-cool, then tempered at 1250°F (677°C) for 2 hours and air-cool. The controlled air-cool from austenite temperature was to obtain a similar percentage ratio of proeutectoid ferrite and bainite as of the original heat treatment. Assuming the casting was 2¾ inch (70 mm) thick, a cooling rate of 54°F per minute (30°C/m) was employed and the resultant ferrite/bainite ratio simulated the original heat treatment very well.

The reheat treated and service-exposed samples were mounted and polished and examined with an optical and microscope SEM. Their hardness was also measured. The findings are summarized in the following.

- Comparing with the restored microstructure, the service-exposed samples showed profound carbide precipitation at grain boundaries, and the extent of the precipitation increased with increasing the service exposure time (Figures 30, 31, 32).

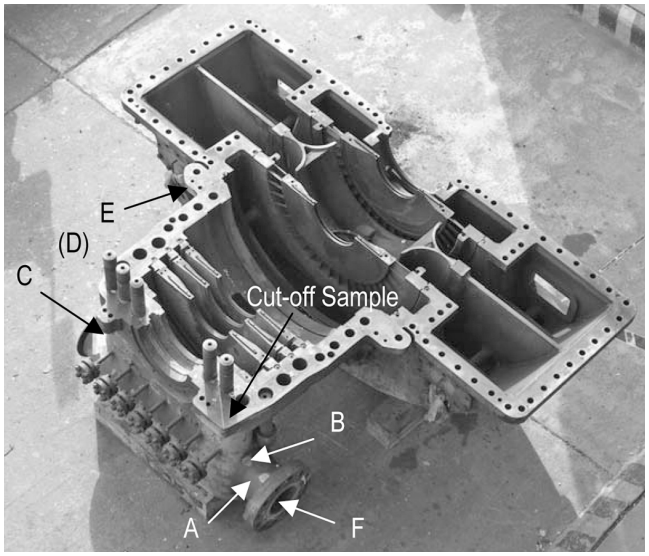

Figure 28. The Turbine Casing and the Replication/Cutoff Locations. F Represented the Hottest Spot, While E Represented the Coolest Spot. D Was at the Transition Radius of Steam Chest to Casing Barrel, Which Was Invisible From this Photo.

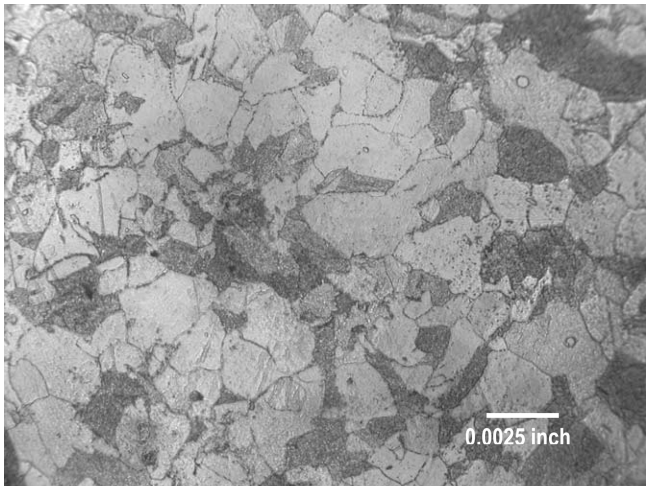

Figure 29. Micrograph of a Replica Taken from Spot D. Carbides Precipitated and Partially Networked at Grain Boundaries. However, No Creep Voids Were Observed There. Five Percent Nital Etched.

Table 4. Casing Hardness Was Fairly Consistent from Spot to Spot.

Spot ID#	Brinell Hardness [HB] (converted from Equotip data)			
	1st Reading	2nd Reading	3rd Reading	Average
A	152	150	155	**152**
B	151	151	156	**153**
C	154	151	153	**153**
D	159	158	159	**159**
E	137	141	140	**139**
F	154	154	154	**154**

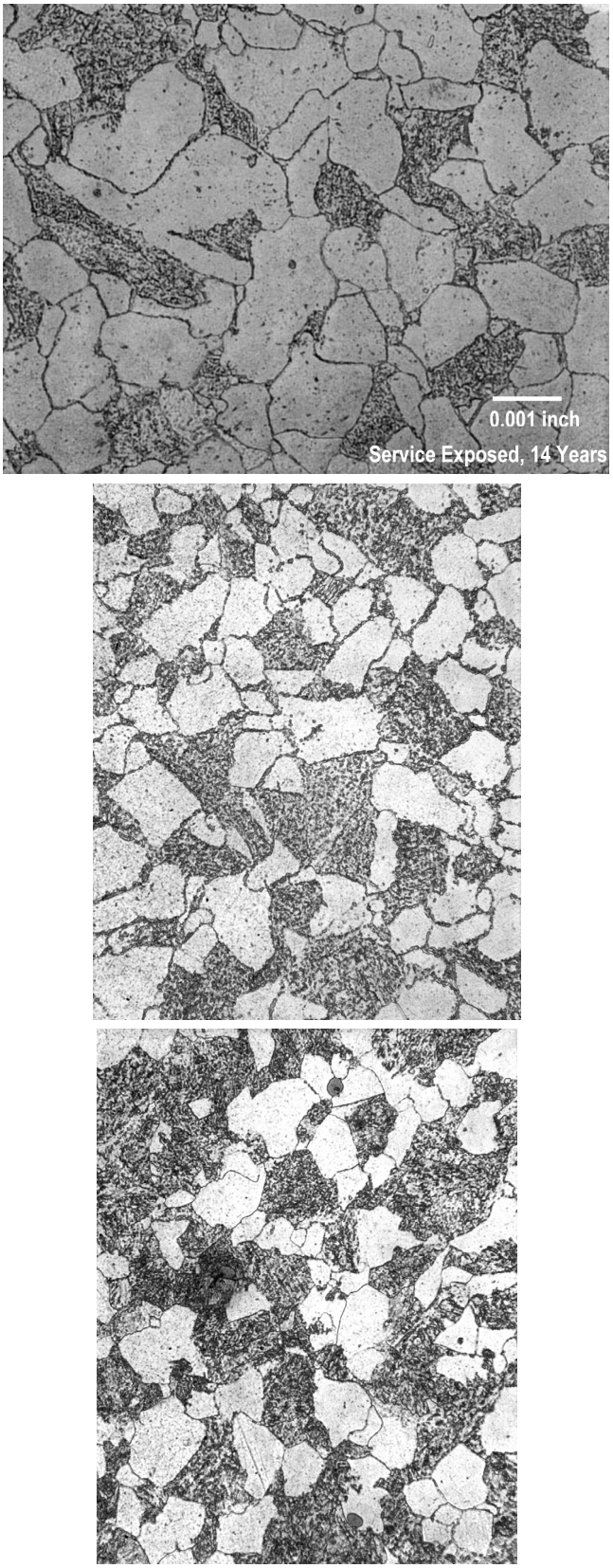

Figure 30. The Extent of Carbide Precipitations at Grain Boundaries Increased with Increasing the Service-Exposure Time. These Precipitations Were the Results of Long-Term Diffusion at Elevated Temperature. A Reheat Treatment (Normalizing Plus Tempering) Generally Restored the Microstructure by Dissolving the Carbides. Five Percent Nital Etched.

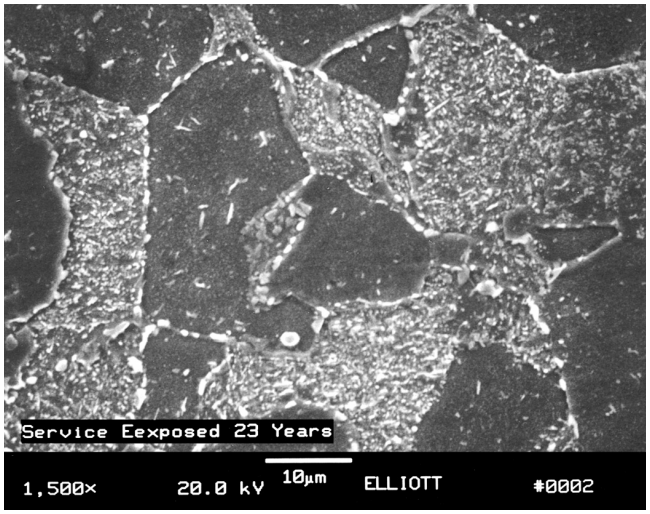

Figure 31. Microstructure of the 23 Years of Service-Exposed Casing Material. Note Deteriorated Bainite and Carbides Precipitated at Grain Boundaries and in Ferrite Phase.

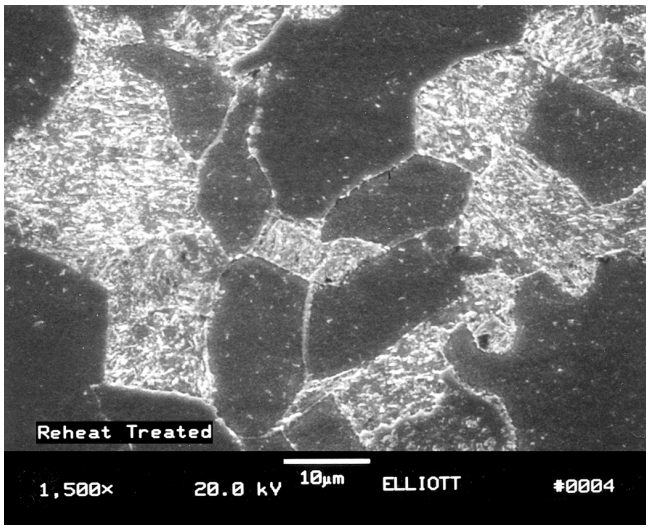

Figure 32. After Being Reheat Treated, the Bainite Phase Was Restored, and the Carbides Were Generally Dissolved.

- Service-exposed samples also showed carbide precipitation inside the proeutectoid ferrite phase.
- Evidence of microstructure degradation of the bainite phase was noticed in the service-exposed sample, due to the transformation of cementite (M_3C) into different carbides (M_2C and M_7C_3).
- No creep voids were found in either sample.
- Hardness was measured as HRB 91 (HB 160) for the service-exposed sample and HRB 93.5 (HB 169) for the reheat treated sample, indicating a slight hardness decrease after a long-term exposure at elevated temperature.

Discussion and Conclusions

Turbine casings usually are normalized and tempered after being cast. This heat treatment leads to a desirable combination of strength/hardness and toughness/ductility for the casing material, 1.25Cr-0.5Mo alloy steel in this case. It also gives an excellent thermal stability for the casings. The typical treatment process contains normalizing at 1685°F (918°C) followed by air-cool then tempering at 1250°F (693°C) followed by air-cool.

The microstructure after the heat treatment consists of proeutectoid ferrite plus bainite. Bainite is a metastable aggregate of ferrite and cementite, which may degrade after long-term exposure at elevated temperature. The degradation was observed as a transformation of cementite (M_3C) into M_2C and M_7C_3 carbides (Biss and Wada, 1985). This transformation will lead to less carbides (in volume percentage) and coarser carbide particles, which will result in lower strength and hardness, which may reduce fatigue and rupture strengths of the material.

Carbon will also diffuse along the grain boundaries and into the proeutectoid ferrite phase to form carbides. Carbides at grain boundaries, especially in networked form, are considered detrimental because they can result in embrittlement and reduce rupture ductility of the material. Another grain boundary damage that is also related to long-term diffusion but was not seen in this case is creep voids. Creep voids are considered as a higher-degree of microstructure damage than the carbide precipitation, and a warning sign of component remaining life.

In the subject turbine casing, no creep voids were evident yet, so the microstructure deterioration was considered moderate and not immediately harmful to the casing life. It was concluded that the casing was in class A condition and could be safely used for the following service period (about five years). However, the microstructure deterioration imposed a concern of the integrity of the casing material and consequent potential risks on the creep strength and rupture ductility of the casings. It was reported that 1.25Cr-0.5Mo low alloy steel could lose its rupture ductility after long-term exposure at elevated temperature (Demirkol, 1999). This behavior is so called rupture ductility trough, which is related to carbides precipitation and may occur before creep voids are developed.

Therefore, in addition to continually monitoring the microstructure with nondestructive replica techniques in the next turnaround, the authors' company suggested that the ethylene plant conduct a Level III remaining life assessment, which requires destructive material tests, in order to evaluate the extent of damage on creep strength and rupture ductility of the casing material. The material tests mainly consist of SRT and CDR test, which are described in a previous section. These two mechanical testings can supply information that microstructure examination (replica) cannot.

CASE STUDY 2— REMAINING LIFE ASSESSMENT OF HOT GAS EXPANDER DISK

A life assessment was performed on a disk from a hot gas expander that had been in operation for approximately 51,000 hours of service. The present life assessment was necessary to ensure that the properties of the disk had not degraded with time. This life assessment consisted of a microstructural evaluation as well as mechanical testing.

Replicas of the microstructure of the disk were taken from five locations shown in Figure 33 and subsequently examined via optical microscope. A blade root from the disk that had seen the same accumulation of time was also sectioned, metallographically prepared using the standard techniques, and examined. Specifically the microstructure was examined in the area of the first, third, and fourth landings. Also specimens were prepared to examine corrosion products.

Representative micrographs of the microstructure of the root of the blade and of the disk may be seen in Figure 34. The structure was found to be uniform and typical for A286 with an ASTM grain size ranging from four to six. No creep voids were observed.

Several areas of high temperature corrosion attack were evident in the area of the first and third root lines of the blade that was sectioned. A micrograph of this corrosion may be seen in Figure 35.

The maximum depth of penetration of corrosion product was found to be approximately 100 micrometers. No corrosion product was observed in areas removed from this accelerated attack, which suggests that a thin Cr_2O_3 layer had formed over the surface of the

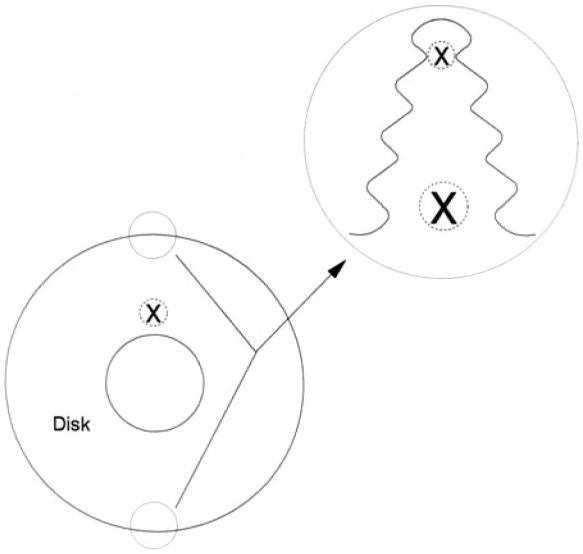

Figure 33. Diagram Indicating Location of Disk Replicas.

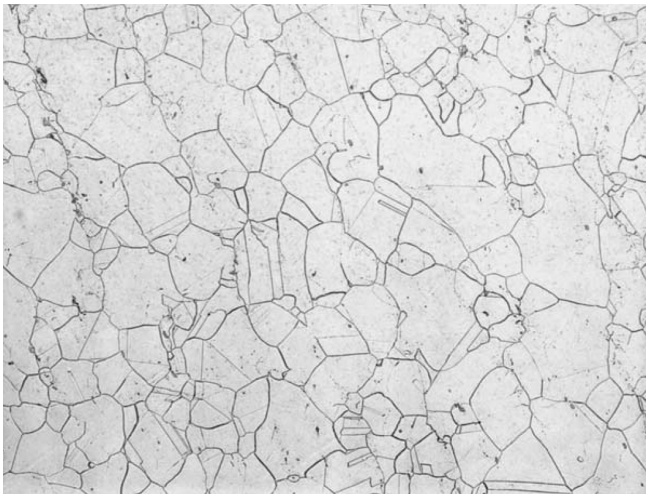

Figure 34. Optical Micrograph of Typical Microstructure of Root of Blade #38. (15 ml HCI, 10 ml HN03, 10 ml Acetic Acid, 100×).

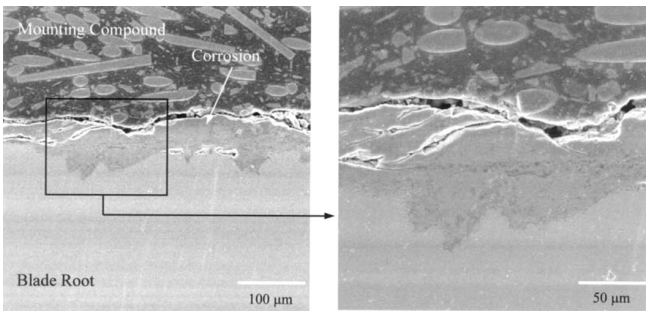

Figure 35. SEM Micrographs of Cross Section of Corrosion Seen in Radius of First Root Landing of Blade #38.

majority of the blade root and remained protective. This type of corrosive attack is expected for an iron chromium based alloy exposed to an atmosphere consisting of a mixture of sulfur and oxygen. Many high temperature alloys including A286 rely on the formation of the compact slow growing chrome oxide scale for protection from the environment. Exposure to sulfur may lead to the breakdown of this protective scale providing the necessary

conditions of temperature and pressure exist. The nature of the corrosive products depends on both thermodynamic and kinetic factors, the details of which are beyond the scope of this paper. A more detailed description of the mixed oxidants is given by Dowson, et al. (1995), and Birks and Meier (1983).

It is not uncommon to see corrosion in the areas of blade root described in Figure 36. One explanation of this is that in these areas there is a gap between the blade root and the disks that allows catalyst into the blade root area. The presence of this catalyst may lead to high temperature corrosion as described by Dowson, et al. (1995), and Dowson and Stinner (2000). Some corrosion was also seen on the context surface of the land that is being proposed that corrosion in these areas is exacerbated by fretting. However, in this investigation this type of corrosion occurred to a much lesser extent than seen in the areas mentioned previously.

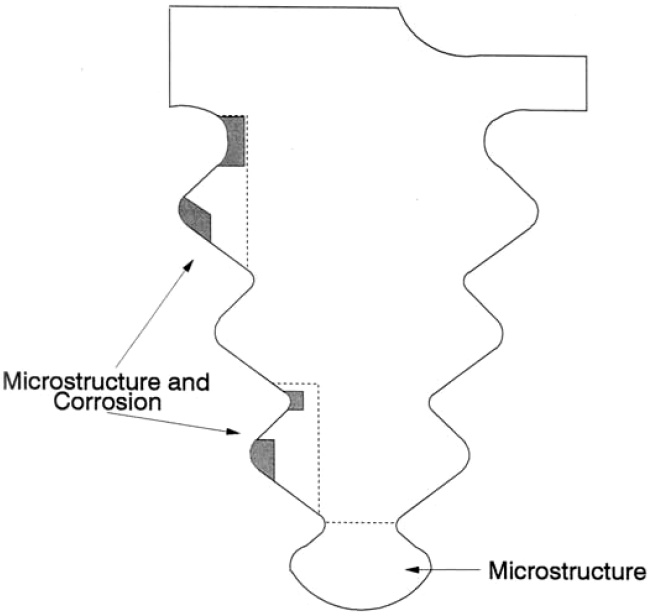

Figure 36. Diagram Indicating Sectioning of Blade Root and Location of Corrosion.

Because destructive testing could not be preformed on the actual disk material, samples for stress rupture testing were taken from the root and lower airfoil of the blade as shown in Figure 37. It was assumed that the properties of the sample are similar to those of the disk roots. Modified stress rupture tests as developed by Dowson, et al. (1995), and Dowson and Stinner (2000) were also performed in order to determine if the corrosion products seen in the blade root area would cause cracking of the disk.

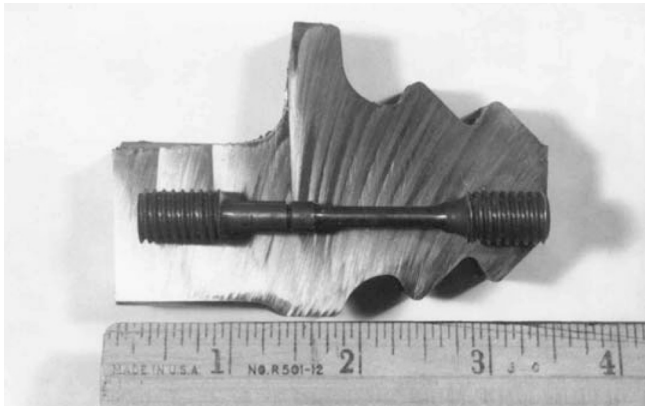

Figure 37. Photograph Illustrating Location from Which Rupture Specimen Was Taken Relative to the Blade Root/Lower Airfoil.

The stress rupture specimen from the blade was found to have an elongation of 10 percent and a reduction of area of 14 percent. The fracture occurred in the smooth section of the bar after 195.5 hours. This meets the authors' company specification, which requires that the specimen last at least 30 hours with rupture occurring in the smooth section and possess an elongation of at least 10 percent. The mill certification of the original blade material gives an elongation and reduction in area of 11.7 and 19 percent, respectively, which is comparable to the present results. Thus, the rupture properties of the disk have not been significantly degraded as a result of operation of the expander.

Modified Stress Rupture Testing

This test developed by Dowson, et al. (1995), is used to determine the stress to cause fracture of the disk material in the presence of spent catalyst. The stress may be converted to a stress intensity that may be compared to the stress intensity at the tip of the "wedge" created by the corrosive product. A determination may then be made as to whether cracking in the disk will occur. It was found that the presence of spent FCC catalyst may greater reduce the rupture strength of Waspaloy®. For example, a sample test of 1200°F and a stress of 95 ksi lasted over 900 hours when tested in air, while the same temperature and stress produced failure in only 3 hours when the sample was tested in the presence of catalyst. In the present investigation, an initial test of 1200°F and a stress of 54 ksi confirmed that A286 is also susceptible to this type of degradation. The sample failed in only 4.25 hours as opposed to 500 hours as predicted by the authors' company material property database for stress rupture in air. Therefore, in order to get an accurate assessment of the rupture properties of the disk in the area of the root in question, the modified stress rupture test was used by Dowson and Stinner (2000). In the case at hand a temperature of 1065 F was chosen for the test based on the temperature of the disk rim at the point of maximum stress, which was determined by finite element analysis to be in the radius of the fourth root landing. The stress used in the tests range from 62 to 102 ksi. Each test consists of an exposure of stress and temperature for at least 20 hours. If the specimen did not break it was unloaded and the catalyst replaced and then retested at a stress that was increased by 10 ksi. This process, which was repeated until fracture occurred at a stress of 102 ksi, corresponds to a stress intensity of 24.27 ksi $\sqrt{inch}$. It should be noted that the catalyst that was used is kept at the authors' company for testing purposes, i.e., it was not from the actual end user's unit. It is likely that this test catalyst was much more contaminated than the end user's catalyst, which will result in lower values of rupture stress than if the actual end user's catalyst was used.

In order to determine the stress intensity of the tip of the corrosion wedge it was first necessary to determine the stress profile. The σ (X) of the area of the root in question, the stress intensity may be calculated from Equation (16):

$$K_I = \int_0^a \sigma(x) m(x,a) dx \tag{16}$$

where a is the wedge depth and the X is the coordinate dimension. The term M (x, a) is the weight function that is dependent on the geometry of the cracked body. When considering the corrosion, wedge formed within the area of a disk rim, the geometry may be approximated as an edge crack in a semi-infinite plate, Equation (17):

$$m(x,a) = \frac{2}{\sqrt{2\pi(a-x)}}\left[1 + .5693\left(1-\frac{x}{a}\right) + .279375\left(1-\left(\frac{x}{a}\right)^2\right)\right] \tag{17}$$

A linearized stress field of the fourth root landing of the disk rim of the end user's expander was determined by a finite element

analysis. From these data an expression of σ (X) was derived and the integral of Equation (16) evaluated to give the stress intensity at the tip of the corrosion wedge. The results of these calculations are summarized in Figure 38, which is a plot of stress intensity versus corrosion wedge depth.

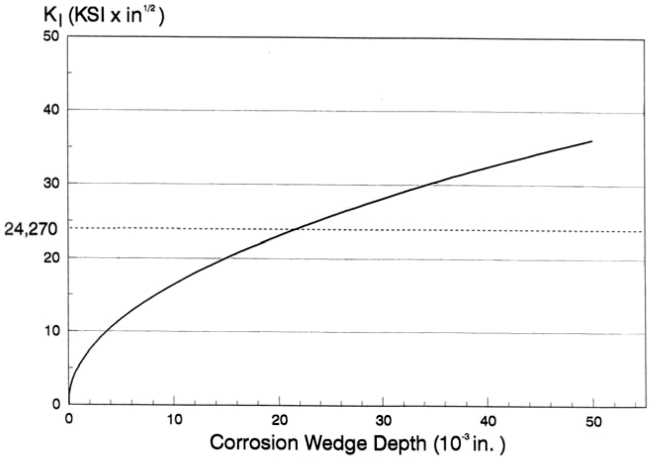

Figure 38. Stress Intensity Versus Corrosion Wedge Depth for Fourth Root Landing of Disk.

Based on this plot, a corrosion wedge will have to penetrate to an approximate depth of .021 inches before the critical stress intensity is exceeded and catastrophic fracture occurs. As mentioned, the maximum penetration seen was approximately .004 inches. Because the growth of the corrosion product is parabolic, e.g., the growth slows with time, it is unlikely that the corrosion would cause a failure of the disk providing the temperature and atmosphere of the expander are not changed significantly.

Conclusions

The microstructure in the ruptured product has not been significantly affected by the operation of the expanders. Some high temperature corrosion was seen in the root area; however, it has been determined that this corrosion will not result in the failure of the disk. Therefore, the disk will be used without significant risk of failure. It is recommended that this be reevaluated after an operational period of four to five years.

REFERENCES

Baik, J. M., Kameda, J., and Buck, O., 1983, *Scripta Met*., 17, p. 1143-1147.

Birks, N. and Meier, G. H., 1983, *Introduction to High Temperature Oxidation of Metals*, London, England: Edward Arnold.

Biss, V. A. and Wada, T., 1985, "Microstructural Changes in 1Cr-0.5Mo Steel after 20 Years of Service," *Metallurgical Transactions A*, *16A*, January, pp. 100-115.

Bruscato, R. M., 1970, "Temper Embrittlement and Creep Embrittlement of 2 °Cr-1 Mo Shielded Metal-Arc Weld Deposits," *Welding Journal*, *35*, p. 148s.

Bush, S. H., 1982, "Failures in Large Steam Turbine Rotors, in Rotor Forgings for Turbines and Generators," R.I. Jaffe, Editor, New York, New York: Pergamon Press, pp. I-1 to I-27.

Carlton, R. G., Gooch, D. J., and Hawkes, B. M., 1967, "The Central Electrical Generating Board Approach to 'The Determination of Remanent Life of High Temperature Turbine Rotors,'" I. Mech E. Paper C300/87.

Demirkol, M., 1999, "On the Creep Strength-Rupture Ductility Behavior of 1.25Cr-0.5Mo Low Alloy Steel," *Journal of Engineering and Environmental Science*, *23*, pp. 389-401.

Dowson, P., 1994, "Fitness for Service of Rotating Turbomachinery Equipment," 10th Annual North American Welding Research Conference, Columbus, Ohio.

Dowson, P., 1995, "Fracture Mechanics Methodology Applied to Rotating Components of Steam Turbines and Centrifugal Compressors," Third International Charles Parson Turbine Conference, Materials Engineering in Turbine and Compressors, *2*, pp. 363-375.

Dowson, P. and Rishel, D. M., and Bornstein, N. S., 1995, "Factors and Preventive Measures Relative to the High Temperature Corrosion of Blade/Disk Components in FCC Power Recovery Turbines," *Proceedings of the Twenty-Fourth Turbomachinery Symposium*, Turbomachinery Laboratory, Texas A&M University, College Station, Texas, pp. 11-26.

Dowson, P. and Stinner, C., 2000, "The Relationship of Stress and Temperature on High-Temperature Corrosion Fracture Mechanics of Waspaloy in Various Catalyst Environments," Proceedings of High Temperature Corrosion and Protection, Materials at High Temperatures, *18*, (2), pp. 107-118.

Foulds, J. R., Jewett, C. W., and Viswanathan, R., 1991, "Miniature Specimen Test Technique for FATT," ASME/1EEE Joint Power Generator Conference, Paper No. 91-JPGC-PWR-38, ASME, New York, New York.

Goldhoff, R. M. and Woodford, D. A., 1972, "The Evaluation of Creep Damage in CrMoV Steel in Testing for Prediction of Material Performance in Structure and Components," STP 515 American Society for Testing and Materials, Philadelphia, Pennsylvania, pp. 89-106.

Kadoya, Y., et al., 1991, "Nondestructive Evaluation of Temper Embrittlement in CrMoV Steel," ASME/JEEE Joint Power Generator Conference, Paper PWR-Vol. 13, New York, New York.

Neubauer, E. and Wadel, V., 1983, "Rest Life Estimation of Creep Components by Means of Replicas," *Advances in Life Prediction Methods*, Editors, Woodford, D. A., and Whitehead, J. E., (New York, New York: ASME), pp. 307-314.

Newhouse D. L., et al., 1972, "Temper Embrittlement of Alloy Steels," ASTM STP 499, pp. 3-36.

Pope, J. J. and Genyen, D. D., 1989, International Conference on Fossil Power Plant Rehabilitation, ASM International, pp. 39-45.

Saxena, A., 1998, "Nonlinear Fracture Mechanics for Engineers," Boca Raton, Florida: CRC Press, p. 449.

Schwant, R. C. and Timo, D. P., 1985, "Life Assessment of General Electric Large Steam Turbine Rotors in Life Assessment and Improvement of Turbogenerator Rotors for Fossil Plants," Viswanathan, R., Editor, New York, New York: Pergamon Press, pp. 3.25-3.40.

Viswanathan, R. and Gehl, S. M., 1991, "A Method for Estimation of the Fracture Toughness of CrMoV Rotor Steels Based on Composition," ASME Transaction, *Journal of Engineering Mat. and Tech*., *113*, p. 263.

Viswanathan, R. and Gehl, S. M., 1992, "Life-Assessment Technology for Power Plant Components," *JOM*, February, pp. 34-42.

Viswanathan, R. and Jaffee, R. J., 1983, "Toughness of Cr-Mo-V Steels for Steam Turbine Rotors," ASME *Journal of Engineering Mat. and Tech*., *105*, pp. 286-294.

Viswanthan R. and Wells, C. H., 1995, "Life Prediction of Turbine Generator Rotors," Third International Charles Parsons Turbine Conference, Materials Engineering in Turbines and Compressors, *1*, pp. 229-264.

Watanabe, J. and Murakami, Y., 1981, "Prevention of Temper Embrittlement of CrMo Steel Vessels by the Use of Low Si Forged Steels," American Petroleum Institute, Chicago, Illinois, p. 216.

Wiegand, R., 1995, "Petroquimica Bahia Blanca Turbine Casing Assessment," An Internal Report.

Woodford, D. A., 1993, *Materials and Design*, *14*, (4), p. 231.

Woodford, D. A., Von Steele, D. R., Amberge, K., and Stiles, D., 1992, "Creep Strength Evaluation for IN738 Based on Stress Relaxation" from *Superalloys*, The Minerals, Metals and Material Society, Editors, Antolovich, S. D., Stusned, R. W., Mackay, R. A., Anton, D. L., Khan, T., Kissinger, R. D., and Klarstrom, D. L., pp. 657-663.

ACKNOWLEDGEMENT

The authors are grateful for the support from the Materials Engineering Department at Elliott Company, and recognize Elliott Company and Dow Chemical PBBPolisur for permission to publish this paper.